

Coupling of intersubband transitions to zone-folded acoustic phonons in a GaN/AlN superlatticeCynthia Aku-Leh,^{1,*} Klaus Reimann,¹ Michael Woerner,¹ Eva Monroy,² and Daniel Hofstetter³¹*Max-Born-Institut für Nichtlineare Optik und Kurzzeitspektroskopie, Max-Born-Strasse 2A, 12489 Berlin, Germany*²*CEA Grenoble, 17 Rue des Martyrs, 38054 Grenoble, France*³*University of Neuchâtel, 1 Rue Abraham Louis Breguet, 2000 Neuchâtel, Switzerland*

(Received 7 February 2012; published 26 April 2012)

Spectrally resolved femtosecond pump-probe measurements of intersubband transitions in a strongly polar GaN/AlN superlattice are presented. A Fourier transform of the data reveals backfolded longitudinal acoustic phonons. The observed phonons couple strongly to the intersubband transitions and modulate the spectral width and position of the intersubband absorption. The coupling is caused by piezoelectric effects and by a phonon-induced modulation of the well width.

DOI: [10.1103/PhysRevB.85.155323](https://doi.org/10.1103/PhysRevB.85.155323)

PACS number(s): 63.20.kd, 78.47.jb, 78.67.De, 73.21.Cd

I. INTRODUCTION

Acoustic phonons are important for heat transfer and energy relaxation processes of carriers in semiconductors. Therefore an understanding of their coupling mechanisms to the carriers is essential both for optoelectronic device performance and fundamental physics. A coupling of acoustic phonons to light requires the simultaneous fulfillment of energy and momentum conservation. Because of the huge ratio between the speed of light and the speed of sound, in bulk materials the coupling is only to phonons with very low frequencies, typically a few gigahertz. In a superlattice, which is formed by alternating layers of two different semiconductors, because of Brillouin zone folding it is possible to have efficient coupling of light to folded acoustic phonons with frequencies of several terahertz.

Folded acoustic phonons in superlattices have been studied extensively¹⁻⁸ in various material systems. In these experiments, the superlattice phonons have been studied via their coupling to interband transitions. In contrast, the coupling of folded phonons to intersubband transitions has up to now received little attention. In one of the very few existing works,⁹ high-frequency longitudinal optical phonons were observed on the wings of the intersubband absorption in a spectrally resolved pump-probe experiment¹⁰⁻¹³ on GaN/AlN heterostructures.

In this article, we show that in a spectrally resolved pump-probe experiment with the pump and probe pulses in resonance with intersubband transition energies we are able to observe folded longitudinal acoustic phonons. The differential transmission signal shows oscillations in its spectral position, its width, and its amplitude either with the frequency of the lowest $q = 0$ folded longitudinal acoustic phonon or with the second harmonic.

II. EXPERIMENT

Our sample is a GaN/AlN superlattice grown by molecular beam epitaxy on a *c*-face AlN-on-sapphire growth template. The superlattice structure consists of 40 alternating layers of 1-nm GaN quantum wells and 2-nm AlN barriers. The underlying 500-nm-thick buffer layer and the 100-nm-thick capping layer are made from Al_{0.65}Ga_{0.35}N. The GaN layers are doped *n*-type with Si to a concentration^{14,15} of $5 \times$

10^{19} cm^{-3} . Since intersubband transitions can only be excited with the electrical polarization parallel to the growth direction, the sample is polished into a symmetric prism shape.¹⁶ A schematic of this geometry is shown as an inset in Fig. 1. A gold layer is evaporated onto the top (see inset of Fig. 1). Light incident on one face of the prism passes through the entire superlattice structure, is reflected back from the gold layer, and passes through the superlattice a second time before leaving the prism. The reflection at the gold layer leads to a standing wave with its antinode at the surface, resulting in a high intensity at the position of the superlattice. In contrast, without the gold layer we have total reflection, resulting in a node at the surface and thus in low intensity at the superlattice. Transmission measurements show an absorption band with a maximum absorption of 75% and a width of 120 meV at 0.968 eV corresponding to the energy separation of the two lowest subbands.

In our experiment, the outputs of two synchronized optical parametric amplifiers¹⁷ (OPA) served as pump and as probe. Both OPAs are seeded by 800-nm, 45-fs-duration pulses from a Ti:sapphire oscillator-amplifier system with a repetition rate of 5 kHz. The pump and probe wavelengths were centered at 1300 nm (0.967 eV) and 1280 nm (0.969 eV), respectively, with *p* polarization at the sample. Both pulse lengths were 80 fs, leading to a width of the cross correlation of 110 fs. After interaction with the sample, the probe beam is spectrally dispersed by a 0.25-m-focal-length spectrometer with a 150 lines per millimeter grating. The spectrum is recorded with a Peltier-cooled InGaAs linear array detector comprising 512 pixels. Measurements were made with the sample at room temperature.

To sensitively determine the pump-induced changes in the probe spectrum, it is necessary to measure simultaneously spectra of the probe pulses with and without the nonlinear interaction in the sample. The reason for this is that there are pulse-to-pulse fluctuations both in the total intensity and in the spectral shape. One (quite expensive) way to measure the two spectra simultaneously is to use two spectrometers and two linear detectors. Instead, we modified a commercial spectrometer by exchanging the normal slit with a double slit. The distance between the two slits is chosen so that the first half of the linear detector is used to measure the spectrum of

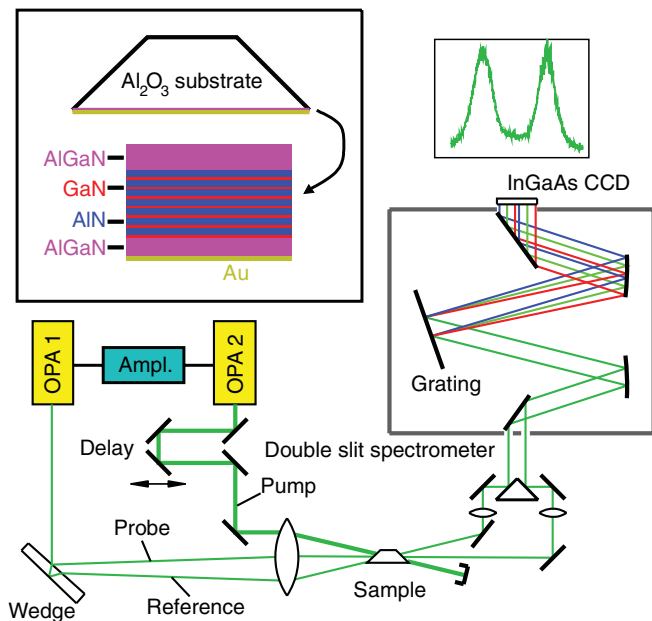


FIG. 1. (Color online) Schematics of our setup and of the sample. Synchronized pump and probe pulses are generated by two optical parametric amplifiers (OPA) pumped by the same Ti:sapphire amplifier. The probe pulses are split into two. Both beams are focused together with the pump pulse onto the superlattice sample. They are then spectrally dispersed in a spectrometer equipped with a double slit and detected by an InGaAs linear array detector (CCD). The inset contains a schematic of the prism-shaped sample used.

light entering through the first slit and the second half is used to measure light entering through the second slit (see Fig. 1). A low-intensity incident probe pulse is split into two pulses by an uncoated wedge. One portion is used as the probe and the other one as a reference beam. Due to the thickness of the wedge of 3 mm the reference pulse is delayed by ~ 30 ps. Together with the pump, both reference and probe pulses are focused onto the superlattice sample, as shown in Fig. 1. Since all pump-induced changes have decayed after 30 ps, the reference spectrum is representative of the unpumped sample. Accordingly, the differential transmission as a function of delay τ and probe wavelength λ is obtained from the difference of the transmitted probe (T_{probe}) and reference (T_{ref}) spectra, normalized by the reference spectrum:

$$\frac{\Delta T}{T}(\lambda, \tau) = \frac{T_{\text{probe}}(\lambda, \tau) - T_{\text{ref}}(\lambda, \tau)}{T_{\text{ref}}(\lambda, \tau)}. \quad (1)$$

III. RESULTS

Figure 2(a) shows normalized differential transmission changes of the probe spectrum in our GaN/AlN superlattice as a function of the pump-probe delay. Maximum transmission changes are on the order of 10^{-2} . The signal before the pump pulse is caused by perturbed free-induction decay and pump-probe coupling¹⁸ (these effects are particularly pronounced in spectrally resolved pump-probe measurements). The data consist of a slowly varying background and superimposed oscillatory features [see Fig. 2(b)]. For the analysis of the

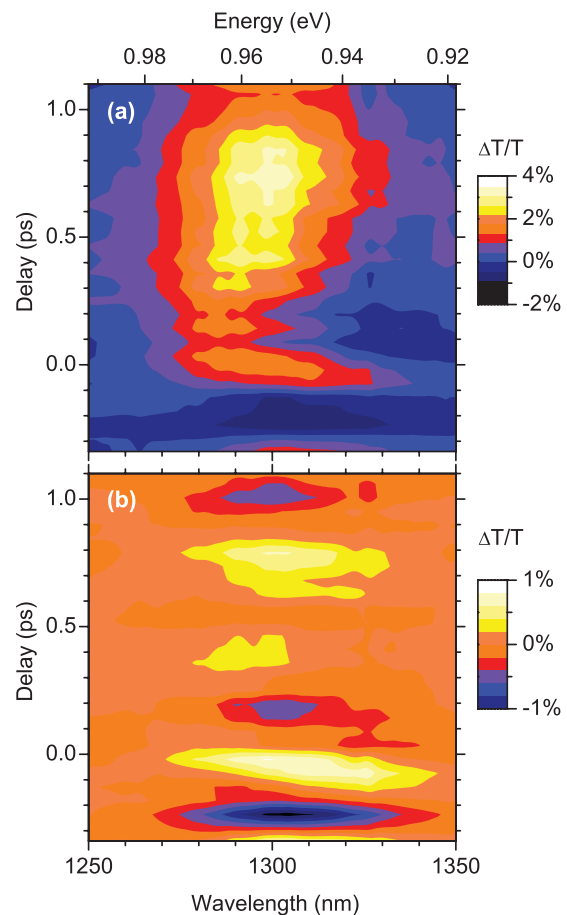


FIG. 2. (Color online) (a) Spectrally resolved differential transmission changes $\Delta T/T$ as a function of pump-probe delay τ and probe wavelength λ . (b) Same data as in panel (a) after removal of the slowly varying background.

data, we fitted Gaussians to the data at every time step:

$$\frac{\Delta T}{T}(\lambda, \tau) = \frac{A(\tau)}{w(\tau)} \exp \left[- \left(\frac{\lambda - \lambda_m(\tau)}{g w(\tau)} \right)^2 \right] + b(\tau). \quad (2)$$

The maximum is at λ_m , b is a constant background, w is the full width at half maximum (FWHM) [$g = 2\sqrt{\ln(2)}$], and A is proportional to the area of the Gaussian. The results of these fits are shown in Figs. 3(a) to 3(c).

The most prominent effect is seen in the position λ_m [Fig. 3(b)]. After the pump pulse, λ_m shifts within the experimental time resolution to shorter wavelengths (higher energies) and recovers afterward. The solid line in Fig. 3(b) is a fit to an exponential decay convoluted with a Gaussian with a FWHM of 110 fs. The time constant obtained is 0.9 ps. From the area and the spectral width [Figs. 3(a) and 3(c)] it is not possible to extract meaningful time constants.

To check for oscillations in the data we have subtracted the slowly varying background [single-exponential fit (solid line) in Fig. 3(b), polynomials in Figs. 3(a) and 3(c)] and then performed a Fourier transform. The spectra obtained are shown in Fig. 3(d). All three spectra, for the position, the width, and the area, have a pronounced peak at 2.8 THz. Additionally, the width and the area have a second peak around 5 THz. The frequency range shown in Fig. 3(d) is limited to 8 THz because

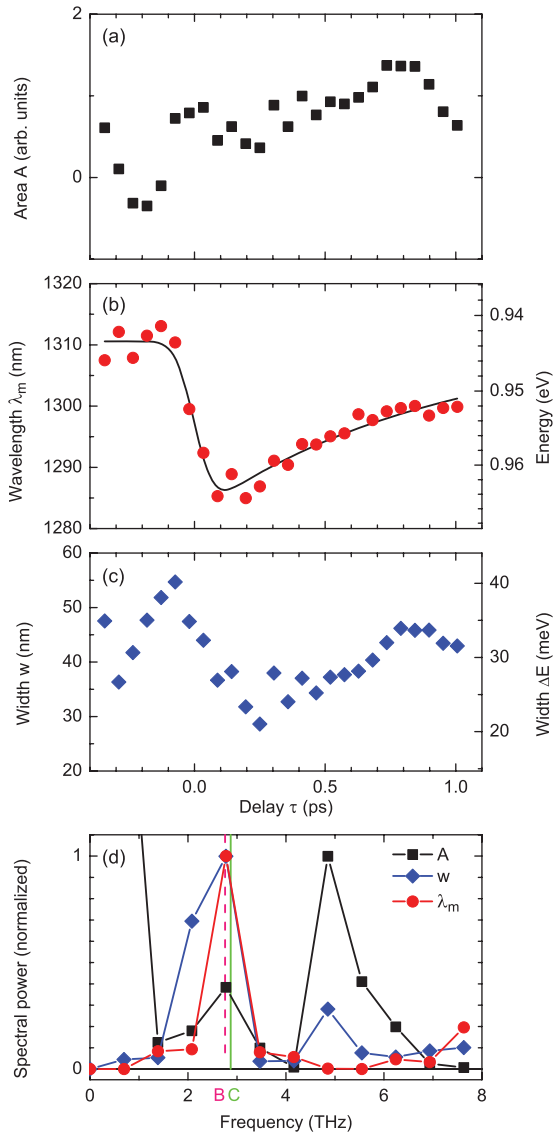


FIG. 3. (Color online) Area (a), spectral position (b), and width (c) of Gaussians fitted to the data shown in Fig. 2(a). The symbols are the results, the solid line in panel (b) is a single-exponential fit convoluted with the cross correlation of pump and probe (Gaussian with a FWHM of 110 fs). (d) Fourier transforms of the results from panels (a) to (c) after subtraction of the slowly varying background. The vertical lines give the frequencies of $q = 0$ folded acoustic phonons (see Fig. 4).

the time resolution in the experiment (110 fs) does not allow the measurement of oscillations with higher frequencies.

IV. DISCUSSION

For positive delays $\tau > 0$, $\Delta T/T(\lambda, \tau)$ is positive, signifying a reduction of the intersubband absorption. The wavelength of the maximum of $\Delta T/T(\lambda, \tau)$ decreases sharply around $\tau = 0$ and recovers afterward with a time constant of 0.9 ps. For the intersubband absorption this corresponds to a shift to lower energies (larger wavelengths) after the pump pulse. There are several mechanisms that lead to such a shift upon pumping. One of these is the depolarization shift,^{19,20}

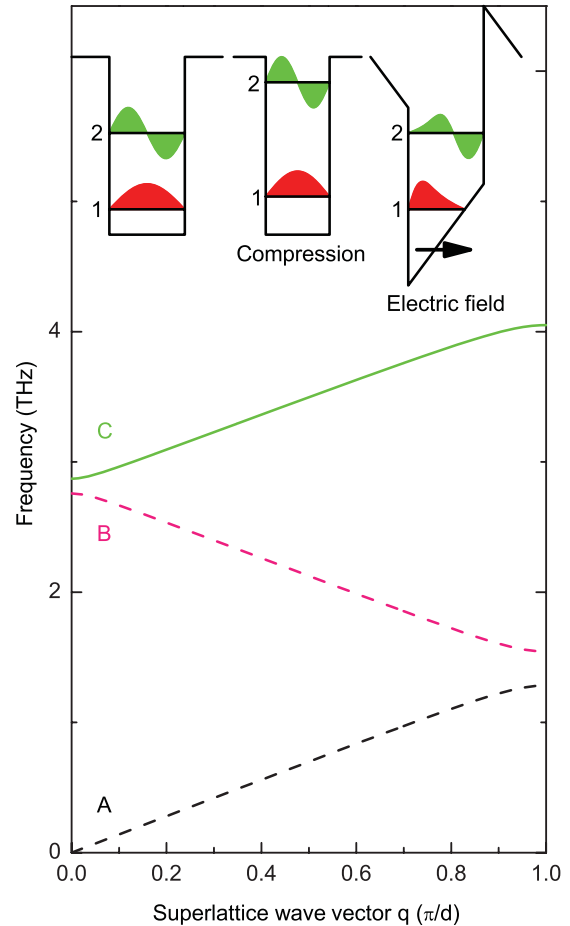


FIG. 4. (Color online) Calculated phonon dispersion curves for a GaN/AlN superlattice with period $d = 3$ nm using the linear chain model. Solid lines represent phonon modes that at $q = 0$ change the thickness of the GaN layers. The insets show schematically the wave functions and the energies relevant for the intersubband transition. On the left there is the unperturbed superlattice. In the middle the well is compressed, leading to an increase of the intersubband transition energy. On the right an electric field distorts the wave functions in the well.

which leads to a blueshift of the absorption compared to the case when no carriers are present. Since this blueshift is proportional to the difference in population between the lower and upper subbands, one expects a decrease of the blueshift upon pumping (and thus a redshift compared to the case where all carriers are in the lower subband). This effect should last for the lifetime of electrons in the upper subband. Previous measurements on a similar superlattice²¹ gave a lifetime of 160 fs, so that the depolarization shift cannot explain the observed wavelength shift at longer delays.

Another effect which causes a wavelength shift upon pumping is carrier heating.²² Because of nonparabolicity, the intersubband absorption of hot carriers will be redshifted compared to cold carriers. This effect will last until the carriers have lost their excess energy to the lattice, for which the observed time constant of 0.9 ps is reasonable.²³

The main result of this article is the observation of oscillations in the time-resolved intersubband absorption. Whereas the observed frequencies of 2.8 and 5 THz are too low for

optical phonons, they agree well with the frequencies of folded acoustic phonons. Since the growth direction of the superlattice is along the c direction, the phonon wave vector also lies along c . Furthermore, one expects a coupling of the intersubband transitions mainly to longitudinal phonons. To calculate the dispersion of these longitudinal acoustic phonons in the superlattice it is sufficient to use a simple linear chain model^{24,25} containing only nearest-neighbor interactions. Since in the c direction GaN (AlN) consists of alternating layers of Ga (Al) and N atoms, longitudinal vibrations lead to a relative movement of adjacent layers, but not to atomic motions within one layer. Therefore, only two force constants are needed, k_{GaN} between Ga and N and k_{AlN} between Al and N. Using the known atomic masses, the force constants are determined from the known longitudinal optic phonon frequencies in the c direction, $\nu_{\text{GaN}} = 22.3$ THz for GaN (Ref. 26) and $\nu_{\text{AlN}} = 26.6$ THz for AlN (Ref. 27), as $k_{\text{GaN}} = 191$ N/m and $k_{\text{AlN}} = 216$ N/m. With the lattice constants²⁸ in the c direction of both GaN and AlN around 0.5 nm, one period (3 nm, consisting of 1 nm GaN and 2 nm AlN) of our superlattice consists of 24 atomic layers. Every second layer contains N atoms. Of the remaining layers, four contain Ga and eight Al atoms. The solutions in the range of folded acoustic phonons of this linear-chain model, using cyclic boundary conditions, are shown in Fig. 4. The observed frequency of 2.8 THz agrees very well with the lowest $q = 0$ folded acoustic phonon. Because of limited frequency resolution, our experiment does not allow the distinction of phonons B and C . Since the coupling mechanisms described below all require a phonon-induced change of the well width, the coupling should be much stronger to phonon C , which leads in contrast to phonon B to a change in well width.

Longitudinal acoustic phonons can couple to intersubband transitions by several mechanisms. One of these is the change of the frequency of the intersubband transition in a superlattice due to a change of the well width. A decrease of the well width leads to an increase of the intersubband frequency (see inset of Fig. 4). Accordingly, if a phonon

leads to an oscillation of the well width, one expects an oscillation of the intersubband frequency with the phonon frequency. Additionally, the intersubband transition dipole moment depends on the spatial extent of the wave functions.

A second mechanism that introduces a coupling between longitudinal phonons and intersubband transitions is the piezoelectric effect, i.e., the generation of an electric field by a compression of the material. This electric field is in addition to the electric field already present in the superlattice.²⁹ Such an electric field, which is directed along the c axis, tilts the confinement potential in the wells (see inset of Fig. 4) and thus influences both the intersubband transition energy and the dipole matrix element.

To determine the relative importance of the two effects we have calculated the change of the transition energies and matrix elements for a fractional change of the GaN layer thickness using the confinement potential from the conduction band offset³⁰ and the built-in electric field.²⁹ For a compression of the GaN layer of 10^{-4} we find a relative change of the intersubband transition energy of 2×10^{-5} from the change of the layer thickness and a change of 2×10^{-4} from the piezoelectric effect. Similarly, the relative change of the dipole matrix element is 7×10^{-6} from the change of the layer thickness and 6×10^{-5} from the piezoelectric effect. Thus, the piezoelectric effect is for both values about ten times larger than the confinement effect.

V. CONCLUSIONS

Using ultrafast spectrally resolved pump-probe measurements we have observed the coupling of intersubband transitions in a GaN/AlN superlattice to folded longitudinal acoustic phonons. The main coupling mechanism is due to piezoelectric fields.

ACKNOWLEDGMENTS

We acknowledge financial support by the Deutsche Forschungsgemeinschaft.

*Present address: ISciences LLC, 2155 Jackson Avenue, Ann Arbor, MI 48103, USA.

¹A. Yamamoto, T. Mishina, Y. Masumoto, and M. Nakayama, *Phys. Rev. Lett.* **73**, 740 (1994).

²A. Bartels, T. Dekorsy, H. Kurz, and K. Köhler, *Phys. Rev. Lett.* **82**, 1044 (1999).

³C.-K. Sun, J.-C. Liang, and X.-Y. Yu, *Phys. Rev. Lett.* **84**, 179 (2000).

⁴V. Y. Davydov, A. A. Klochikhin, I. E. Kozin, V. V. Emtsev, I. N. Goncharuk, A. N. Smirnov, R. N. Kyutt, M. P. Scheglov, A. V. Sakharov, W. V. Lundin, E. E. Zavarin, and A. S. Usikov, *Phys. Status Solidi A* **188**, 863 (2001).

⁵M. Bargheer, N. Zhavoronkov, Y. Gritsai, J. C. Woo, D. S. Kim, M. Woerner, and T. Elsaesser, *Science* **306**, 1771 (2004).

⁶C. E. Martinez, N. M. Stanton, P. M. Walker, A. J. Kent, S. V. Novikov, and C. T. Foxon, *Appl. Phys. Lett.* **86**, 221915 (2005).

⁷M. Bargheer, N. Zhavoronkov, J. C. Woo, D. S. Kim, M. Woerner, and T. Elsaesser, *Phys. Status Solidi B* **243**, 2389 (2006).

⁸C.-Y. Chen, Y.-C. Wen, H.-P. Chen, T.-M. Liu, C.-C. Pan, J.-I. Chyi, and C.-K. Sun, *Appl. Phys. Lett.* **91**, 133101 (2007).

⁹Z. Wang, K. Reimann, M. Woerner, T. Elsaesser, D. Hofstetter, J. Hwang, W. J. Schaff, and L. F. Eastman, *Phys. Rev. Lett.* **94**, 037403 (2005).

¹⁰W. T. Pollard and R. A. Mathies, *Annu. Rev. Phys. Chem.* **43**, 497 (1992).

¹¹C. H. Brito Cruz, R. L. Fork, W. H. Knox, and C. V. Shank, *Chem. Phys. Lett.* **132**, 341 (1986).

¹²G. Stock and W. Domcke, *Chem. Phys.* **124**, 227 (1988).

¹³K. Adamczyk, M. Prémont-Schwarz, D. Pines, E. Pines, and E. T. J. Nibbering, *Science* **326**, 1690 (2009).

¹⁴D. Hofstetter, S.-S. Schad, H. Wu, W. J. Schaff, and L. F. Eastman, *Appl. Phys. Lett.* **83**, 572 (2003).

- ¹⁵D. Hofstetter, E. Baumann, F. R. Giorgetta, M. Graf, M. Maier, F. Guillot, E. Bellet-Amalric, and E. Monroy, *Appl. Phys. Lett.* **88**, 121112 (2006).
- ¹⁶F. Eickemeyer, M. Woerner, A. M. Weiner, T. Elsaesser, R. Hey, and K. H. Ploog, *Appl. Phys. Lett.* **79**, 165 (2001).
- ¹⁷R. A. Kaindl, M. Wurm, K. Reimann, P. Hamm, A. M. Weiner, and M. Woerner, *J. Opt. Soc. Am. B* **17**, 2086 (2000).
- ¹⁸M. Chachisvilis, H. Fidler, and V. Sundström, *Chem. Phys. Lett.* **234**, 141 (1995).
- ¹⁹T. Ando, A. B. Fowler, and F. Stern, *Rev. Mod. Phys.* **54**, 437 (1982).
- ²⁰S. Graf, H. Sigg, K. Köhler, and W. Bächtold, *Phys. Rev. Lett.* **84**, 2686 (2000).
- ²¹Z. Wang, K. Reimann, M. Woerner, T. Elsaesser, D. Hofstetter, E. Baumann, F. R. Giorgetta, H. Wu, W. J. Schaff, and L. F. Eastman, *Appl. Phys. Lett.* **89**, 151103 (2006).
- ²²R. A. Kaindl, M. Wurm, K. Reimann, M. Woerner, T. Elsaesser, C. Miesner, K. Brunner, and G. Abstreiter, *Phys. Rev. Lett.* **86**, 1122 (2001).
- ²³J. Hamazaki, H. Kunugita, K. Ema, A. Kikuchi, and K. Kishino, *Phys. Rev. B* **71**, 165334 (2005).
- ²⁴M. Born and K. Huang, *Dynamical Theory of Crystal Lattices* (Oxford University Press, London, 1954).
- ²⁵C. Colvard, T. A. Gant, M. V. Klein, R. Merlin, R. Fischer, H. Morkoc, and A. C. Gossard, *Phys. Rev. B* **31**, 2080 (1985).
- ²⁶A. S. Barker and M. Ilegems, *Phys. Rev. B* **7**, 743 (1973).
- ²⁷J. A. Sanjurjo, E. López-Cruz, P. Vogl, and M. Cardona, *Phys. Rev. B* **28**, 4579 (1983).
- ²⁸H. Schulz and K. H. Thiemann, *Solid State Commun.* **23**, 815 (1977).
- ²⁹O. Ambacher, J. Smart, J. R. Shealy, N. G. Weimann, K. Chu, M. Murphy, W. J. Schaff, L. F. Eastman, R. Dimitrov, L. Wittmer, M. Stutzmann, W. Rieger, and J. Hilsenbeck, *J. Appl. Phys.* **85**, 3222 (1999).
- ³⁰G. Martin, A. Botchkarev, A. Rockett, and H. Morkoç, *Appl. Phys. Lett.* **68**, 2541 (1996).